RSC Advances

ROYAL SOCIETY OF CHEMISTRY

www.rsc.org/advances

Rationally designed hierarchical $ZnCo_2O_4$/Polypyrrole nanostructures for high-performance supercapacitor electrodes

Tingting Chen[a,b], Yong Fan*[a], Guangning Wang [a,b], Qing Yang[b], and Ruixiao Yang[a]

Abstract

Electrodes with rationally designed hybrid nanostructures can offer many opportunities for the enhanced performance in electrochemical energy storage. In this work, hierarchical $ZnCo_2O_4$/Polypyrrole (PPy) nanostructures on Ni foam were rationally designed and successfully fabricated through a facile two-step method and were directly used as an integrated electrode for supercapacitors. The novel nanoscale morphology has been proven to be responsible for their excellent capacitive performances. When used as electrodes in supercapacitors, the hybrid nanostructures demonstrated prominent electrochemical performances with a high specific capacitance (1559 F/g at a current density of 2 mA/cm^2), a good rate capability (89% when the current density increases from 2 to 20 mA/cm^2), and a good cycling ability (90% of the initial specific capacitance remained after 5000 cycles at a high current density of 10 mA/cm^2). Moreover, the high specific energy density is 30.9 Wh/kg at a current density of 2 mA/cm^2 in a two-electrode system. The excellent electrochemical performance of hierarchical $ZnCo_2O_4$/PPy nanostructures can be mainly ascribed to the enhanced adherent force between electrode materials and Ni foam to hold the electrode fragments together by means of $ZnCo_2O_4$ nanowires, the good electrical conductivity of PPy, the short ion diffusion pathway in ordered porous PPy nanofilms and $ZnCo_2O_4$ nanowires.

Key Words: Polypyrrole; $ZnCo_2O_4$; Hierarchical Structure; Supercapacitor; Cycling Performance.

---

[a] *The College of Material Science and Engineering, Harbin University of Science and Technology, Harbin, 150040, P. R. China.*

[b] *The Key Laboratory for Photonic and Electronic Bandgap Materials, Ministry of Education, School of Physics and Electronic Engineering, Harbin Normal University, Harbin, 10025, P. R. China.*

**Corresponding author E-mails: fyzf318@163.com*

† Electronic supplementary information (ESI) available: (Fig. S1) SEM and TEM images, and (Fig. S2) mapping images of hybrid nanostructures; The CV curves and GCD curves of PPy and $ZnCo_2O_4$ (Fig. S3); GCD curves of the PPy, $ZnCo_2O_4$, and $ZnCo_2O_4$/PPy (Fig. S4); The data of Specific capacitance (Table S1); The CV curves and GCD curves of PPy and $ZnCo_2O_4$ in a two electrode system (Fig. S5).

Introduction

In recent years, owing to increasing concern about the rapid depletion of fossil fuels and increasingly worsened environmental pollution, energy storage is becoming one of the great challenges to maintain a healthy, prompt and sustainable economic development. As the novel devices for energy storage, supercapacitors distinguish from other types of electrochemical energy storage by their advantages of short charging times, good reversibility, high power density, and long cycle life, which have attracted increasing attention in past decades.[1,2] Supercapacitors can be divided into electrical double layer capacitors and pseudocapacitors (PCs) according to the charge storage mechanisms.[3] In particularly, capacitance of PCs arises from the fast reversible Faradic redox reactions at the electrode surface, thus PCs usually provide much higher specific capacitance than supercapacitors made of carbonaceous materials based on electric double-layer charge storage.[4,5] Thus, a number of current studies have been focused on PCs.

Since the first report of electrical conductivity in a conjugated polymer in 1977 was presented by H. Shirakawa et al[6]., conducting polymers have received much attention because they combine the electrical properties of metals and the advantages of polymers.[7] Among the conducting polymers for the PCs, polypyrrole (PPy) is one of the most promising conducting polymers for supercapacitors[8-9] because of its high conductivity (10−100 S/m)[10], facile preparation, good thermal and environmental stability, environment friendly, flexibility, high redox and capacitive current.[11] However, it has a relatively poor cycling stability and rate capability, because large volumetric swelling and shrinking during charge/discharge process as a result of ion doping and dedoping.[12] This volumetric alternation often leads to structural breakdown and thus fast capacitance decay of conducting polymers.[13,14] Apparently, most PPy-based electrode retain less than 50% of the initial capacitance after cycling for 1000 times. PPy/carbon prepared by An et al.[11] presented high specific capacitance (433 F/g at 1 mV/s), but poor cycling stability 36% after 2000 cycles at 1 A/g. Therefore, cycling instability and rate capability is a major obstacle for practical

applications of conductive polymer electrodes. Recently, much effort has been focused on the development of hybrid nanomaterials based on PPy in order to improve the stability, such as metal-polypyrrole core-shell nanoparticles and metal-polypyrrole hybrid nanowires.[15–18] In these hybrid materials, metal nanoparticles functions as a skeleton for docking electroactive materials that can hold the electrode fragments together, and improve the stability of PPy. Particularly, $ZnCo_2O_4$ exhibits a higher stability than that of PPy materials.[19-24] $ZnCo_2O_4$ nanowire prepared by Li et al.[25] presented excellent cycling stability 90% after 6000 cycles at 20 mA/cm^2. In this sense, nanostructured $ZnCo_2O_4$ is considered to be an excellent skeleton for docking electroactive materials. For example, Chuo et al.[26] take full advantage of $ZnCo_2O_4$ to enhance the adhere force between electrodes and Ni foam to improve the stability of $Ni(OH)_2$, in which the $ZnCo_2O_4$ nanowires act as the backbone and provide "superhighway" for electron, in addition, the $ZnCo_2O_4$ nanowires can solidify electrode materials to Ni foam and thus avoids electrode materials to fall off. These works imply that it might be possible to fabricate the hybrid electrode of $ZnCo_2O_4$/PPy with excellent electrochemical performance.

Based on the considerations above, in this work, we have designed porous hierarchical $ZnCo_2O_4$/PPy hybrid nanostructures on Ni foam. This electrode design has many apparent advantages such as: (1) The highly porous $ZnCo_2O_4$ nanowires directly grown on conductive Ni foam can enhance the adhere force between electrode materials and substrate to hold the electrode fragments together, and improve the stability of PPy. (2) The high electrical conductive PPy, which has the smaller internal resistances and diffusion resistance, led to enhanced electrochemical activity of $ZnCo_2O_4$/PPy hybrid materials. Intimately covered PPy increases both the electrical conductivity of each $ZnCo_2O_4$ nanowire and the electrical contact of $ZnCo_2O_4$ with nickel foam current collector, leading to the maximum utilization of $ZnCo_2O_4$ during the electrochemical reactions. (3) The porous $ZnCo_2O_4$ nanowires and porous PPy nanofilms growing onto the $ZnCo_2O_4$ nanowires have a high surface area and provide more active reaction sites, improving the utilization of active

materials not only on the active material surface but also throughout the bulk. (4) The wire structure and the large open space between the nanofilms can greatly enhance the kinetics of ion and electron transport inside the electrodes. The abundant space between individual nanostructures allows for facile diffusion of electrolyte into inner region of the electrode.

Experiments

In the experiment, all the reagents were of analytical grade and used without any further purification.

Synthesis of $ZnCo_2O_4$ nanowires: Before the fabrication of $ZnCo_2O_4$ samples, the nickel foam substrate was treated with 6 M HCl in an ultrasound for 20 min to remove the oxide layer, and then rinsed with deionized water for 30 min .In a typical synthesis, $Zn(NO_3)_2 \cdot 6H_2O$ (1 mmol, 0.297 g), $Co(NO_3)_2 \cdot 6H_2O$ (2 mmol, 0.582 g), $CO(NH_2)_2$ (5 mmol, 0.300 g) and NH_4F (2 mmol, 0.074 g) were added together into 40 mL deionized water under stirring, forming a clear red solution. Sequentially, the mixed solution and a piece of pretreated Ni foam were transferred together into a capacity of 50 mL Teflon-lined stainless steel autoclave, heated in an oven at 120 ℃ for 5 h, and then cooled down to ambient temperature naturally. The Ni foam coated with a pink product was taken out from the autoclave and rinsed carefully with deionized water, then annealed in an oven at 400 ℃ for 2 h.

Synthesis of hierarchical $ZnCo_2O_4$/PPy nanostructures: The hybrid nanostructures were obtained by electrodeposition with a Lab-logic electrochemical workstation (VMP3, France). Primarily, $ZnCo_2O_4$ nanowires was immersed in pyrrole/acetone solution with a concentration of 0.5 M for 0.5 h. Then, the $ZnCo_2O_4$ nanowires with pyrrole (Py) monomers adsorbed on the surface of each individual $ZnCo_2O_4$ nanowires was directly used as the working electrode under a potential of 0.8 V in 0.3 M $LiClO_4$ aqueous solution. A Pt wire and Ag/AgCl were used as the counter and reference electrodes, respectively. A typical electropolymerization time was 5 min.

After the electropolymerization process, the hierarchical $ZnCo_2O_4$/PPy nanostructures were obtained. The nickel foam supported hybrid nanostructure (~1.5 cm^2 area; $ZnCo_2O_4$ mass: 1.426 mg; PPy mass: 1.434 mg) or pristine $ZnCo_2O_4$ nanowires acted directly as the working electrode. Pure PPy were deposited on Ni foam for 5 minutes in order to have the same thickness of PPy with the hierarchical $ZnCo_2O_4$/PPy nanostructures.

The sample morphology and structure of the nanocomposites were characterized by scanning electron microscopy (SEM, Hitachi SU 70) 、Transmission electron microscopy (TEM; FEI, Tecnai TF 20) 、Fourier transform infrared (FTIR, BRUKER VERTEX 80) and X-ray diffraction (XRD; D/max-2600/PC, Rigaku, Japan) with Cu Kα radiation (λ = 1.5418 Å) in the 2θ of 20–70°.

The electrochemical properties were measured on a Lab-logic electrochemical workstation (VMP3, France) using a three-electrode configuration in 3 M KOH, where the $ZnCo_2O_4$/PPy nanostructure served as working electrode, a platinum plate and Ag/AgCl as the counter and reference electrodes, respectively. Cyclic voltammetry (CV) tests were recorded from -0.1 to 0.58 V at scan rates of 5, 15, 25, and 40mV/s at room temperature. The galvanostatic charge/discharge (GCD) property was measured at the current densities of 2, 5, 10, 15, and 20 mA/cm^2 with the potential in range of 0 to 0.44 V. Electrochemical impedance spectroscopy (EIS) measurements were carried out on this apparatus in the frequency range of 100 kHz to 10 mHz. The specific capacitance (Cs), area capacitance (Ca) was calculated using the following equation：

$$C_s = \frac{I\Delta t}{m\Delta V} \qquad (1)$$

$$C_a = \frac{I\Delta t}{SV} \qquad (2)$$

In a two-electrode system, the specific energy (E) and the specific power (P) was

calculated using the following equation：

$$E = \frac{1}{2} \times \frac{C_s}{4} \times \Delta V^2 \quad (3)$$

$$P = \frac{E}{\Delta t} \quad (4)$$

where C (F/g) is specific capacitance , I(A) is the current during the discharge process, Δt (s) is the time of discharge, ΔV(V) is the voltage difference between the upper and lower potential limits, and m (g) is the mass of the electrode materials.

Results and discussion

The representative synthetic procedure of the hybrid nanostructures electrode is illustrated in Fig. 1. First, commercial nickel foam was employed as the current collector to grow $ZnCo_2O_4$ nanowire via a modified hydrothermal and annealing process. Then, the $ZnCo_2O_4$ nanowire was immersed into a Py solution to adsorb a layer of Py molecules on the nanowire surface. Finally, the Py monomers were crosslinked into a solid PPy layer by electropolymerization in a three-electrode cell with the sponge as the working electrode. Fig. 2a shows typical SEM images of the as-synthesized $ZnCo_2O_4$ nanowires on Ni foam. Fig. 2b is the enlarged SEM image of a local area in the Fig. 2a. From the magnified SEM image, it can be seen, that the nanowires have an average diameter of 40 nm and the length is about 7 μm. The further magnified view in the Fig. 2c shows the porous structure of $ZnCo_2O_4$ nanowires, which can be due to the release of gas during the calcining process.[27,28] Fig. 2d demonstrates a representative low-magnification SEM image of the hierarchical $ZnCo_2O_4$/PPy nanostructures. Fig. 2e shows a magnified SEM image of the local area in the Fig. 2d. Obviously, the $ZnCo_2O_4$ nanowires uniformly pass through the PPy nanofilms to form nanoarray network. From the magnified SEM image in the Fig. 2f, it can be found that porous PPy nanofilms were deposited onto the surface of $ZnCo_2O_4$ nanowires. The porous nanostructure of PPy was formed by the oxidation

and reduction process of the polymer during its growth progress.[29] Such a unique nanoarray network nanostructure has open and free interspaces among themselves (Fig. S1a†), which assures that electrolytes are highly accessible to all the electrode materials and then could improve the utilization rate of electrode materials, thus providing more surface area for easy diffusion of the electrolyte into the inner interface of the electrode materials.

The microstructures of the $ZnCo_2O_4$ and $ZnCo_2O_4$/PPy hybrid nanostructures were further investigated using TEM. Fig. 3a shows a TEM image of a single $ZnCo_2O_4$ nanowire with a diameter of ~40 nm that further confirms the presence of the highly porous structure, which is consistent with SEM observation. Fig. 3b shows a HRTEM image of the porous $ZnCo_2O_4$ nanowire. It reveals an interplanar spacing of 0.29 nm and 0.25 nm, corresponding to the (220) and (311) lattice planes of $ZnCo_2O_4$. The typical TEM image of the hierarchical $ZnCo_2O_4$/PPy nanostructure is shown in Fig. 3c. It is evidently observed that the $ZnCo_2O_4$ is shelled by an amorphous PPy layer, forming a typical core−shell structure. The HRTEM examination shown in Fig. 3d reveals the amorphous PPy layer with the thickness of more than ten nanometers. In addition, some PPy nanofilms are attached tightly to the nanowire in the particulate form with visibly larger sizes, as shown in Fig. S1b†. TEM image of the hierarchical $ZnCo_2O_4$/PPy nanostructure shows that PPy is either immobilized onto the surface of $ZnCo_2O_4$ nanowires as a nanosized thin layer or firmly attached to the nanowires in the form of nanofilms, and the two kinds of existing PPy in the hybrid structure would definitely facilitate the electron transport and enhance the electrical connection with the current collector.[30] These features enable our hybrid electrode to satisfy the critical requirements for electrochemical capacitors. Moreover, it is clearly shown in Fig. S2† that the elements N, C, O, Co, and Zn are homogeneously distributed, achieving the uniform coating of PPy on the $ZnCo_2O_4$ NWs.

The Fourier transform infrared spectroscopy (FTIR) spectrum provides further evidence for the presence of PPy (Fig. 3e). In detail, the first broad band located at

3346 cm^{-1} corresponds to N–H bonds of aminegroups.[30] The two peaks at 2968 and 2872 cm^{-1} correspond to aliphatic C–H groups.[31] The peak observed at 2357 cm^{-1} is associated with the hydroxyl vibration.[32] The peak at 1408 cm^{-1} is due to the =C−H in-plane vibration, the band at 1089 cm^{-1} is characteristic of the C−N stretching vibration , and the band at 1012 cm^{-1} is attributed to C–H and N–H in-plane ring deformation vibration.[33-35] The slight shift of the FTIR peaks of PPy is considered to arise from the interfacial interaction between PPy and $ZnCo_2O_4$. A typical XRD pattern of the $ZnCo_2O_4$ and $ZnCo_2O_4$/PPy hybrid nanostructures are shown in Fig. 3f. The diffraction peaks of pure $ZnCo_2O_4$ can unambiguously demonstrate the structure of face-centered cubic $ZnCo_2O_4$ (JCPDS card no. 23-1390). It can be observed that the XRD pattern of $ZnCo_2O_4$/PPy hybrid nanostructures has a similar XRD pattern of $ZnCo_2O_4$. However, different from the peak of $ZnCo_2O_4$, the peak of $ZnCo_2O_4$/PPy hybrid nanostructures exhibits another broad reflection located in the range of 20-30°, which is attributed to the diffraction patterns of amorphous PPy.[36] On the basis of the characterizations above, it can be confirmed that the PPy was successfully coated on the surface of the nanowires.

In order to explore the electrochemical properties of $ZnCo_2O_4$/PPy hybrid nanostructures, both CV and GCD cycling measurement were carried out with 3 M KOH aqueous solution in a three-electrode system. As shown in Fig. 4a, the enclosed area of the $ZnCo_2O_4$/PPy hybrid electrode is obviously larger than that of $ZnCo_2O_4$ and PPy. This increased area is mainly contributed by synergistic effects[36] between $ZnCo_2O_4$ and PPy. The CV and GCD measurements of the PPy and $ZnCo_2O_4$ electrodes were performed at various scan rates and various current densities to compare the electrochemical activities (Fig. S3†). From the obtained GCD profiles of the three electrodes as shown in Fig. S4†, the C_s of the hybrid electrodes, $ZnCo_2O_4$ nanowire electrodes and PPy electrodes are calculated to be 1559 F/g, 1275 F/g, and 180 F/g, respectively. The value of $ZnCo_2O_4$/PPy hybrid electrode is higher than that of $ZnCo_2O_4$ and PPy. The larger C_s for $ZnCo_2O_4$/PPy is due to the improvement of the electronic conductivity between the particles, owing to their PPy coat. Fig. 4b shows

the CV curves of the $ZnCo_2O_4$/PPy hybrid nanostructures supported on Ni foam at various scanning rates ranging from 5 to 40 mV/s. Obviously, a pair of distinct redox peaks are visible in the CV curves with the potential windows ranging from -0.1 to 0.58 V, demonstrating that the capacitance characteristics are mainly ascribed to the faradic capacitive behavior. Interestingly, the redox current almost linearly increases with increasing scan rate, demonstrating that the kinetics of interfacial Faradic redox reactions and the rate of electronic and ionic transport are rapid enough.[37] And also, the reduction and oxidation peaks slightly shift toward lower and higher potential, respectively, which can be attributed to the polarization effect of the electrode.[38]

To estimate the specific capacitance of the $ZnCo_2O_4$/PPy as supercapacitor electrodes, GCD measurements were further performed at various current densities of 2, 5, 10, 15 and 20 mA/cm^2. As shown in Fig. 4c, the potential plateaus in the discharge curves match well with the reduction peaks observed in the CV curves, which correspond to the reductive process, and this phenomenon indicates good pseudocapacitive behaviors. The Cs of PPy, $ZnCo_2O_4$ and $ZnCo_2O_4$/PPy hybrid electrodes at various current densities are shown in Fig. 4d. The corresponding calculated values are provided in Supporting Information. The Cs measured in the same way is reported in Table S1†. The Cs of the $ZnCo_2O_4$/PPy hybrid electrodes are calculated to be 1559, 1500, 1442, 1414, and 1388 F/g at current densities of 2, 5, 10, 15, and 20 mA/cm^2, respectively, according to formula (1). The Cs decreases when the current density increases, which reflects the loss of efficiency of the active material at high current densities. The corresponding Ca is 2.54, 2.50, 2.43, 2.39, and 2.35 F/cm^2, respectively, according to formula (2). Most importantly, the Cs of the $ZnCo_2O_4$/PPy hybrid electrodes still keeps at 1388 F/g at a high density of 20 mA/cm^2, 89 % of that at 2 mA/cm^2, highlighting the excellent rate capability of the $ZnCo_2O_4$/PPy hybrid electrodes. It can be noted that the capacitance retention is 53.3%, 73.8%, and 89% as the current density is increased from 2 to 20 mA/cm^2 for PPy, $ZnCo_2O_4$ and $ZnCo_2O_4$/PPy, respectively. The rate capability of the $ZnCo_2O_4$/PPy electrodes is better than that of PPy and $ZnCo_2O_4$, as well as many other pseudocapacitor

electrodes such as PPy@C[39] (19.5% Areal capacitance retention from 2 mA/cm^2 to 10 mA/cm^2)、activated carbon/PPy[40] (71.4% capacitance retention from 2 mA/cm^2 to 20 mA/cm^2)、V_2O_5/PPy nanostructures[41] (about 73% capacitance retention from 2 A/g to 10 A/g)、$ZnCo_2O_4$ Nanorods[42] (83% capacitance retention from 2 A/g to 20 A/g).

The durability of the electrode materials is a critical aspect for supercapacitor applications. The cycling performance was conducted in the potential windows ranging from 0 to 0.44 V. Fig. 4e shows the cycling performance of 5000 cycles at a current density of 10 mA/cm^2 of PPy, $ZnCo_2O_4$ and $ZnCo_2O_4$/PPy. During the first 1400 cycles at 10 mA/cm^2, the Cs was increasing, and then decreasing during the last 3600 cycles and finally maintained at about 90% after 5000 cycles. The increasing Cs can be mainly attributed to the activation process of the active materials in the electrolyte.[43] With the cycle number increasing, the ions of electrolyte first go through PPy, and then diffuse to the inter $ZnCo_2O_4$ absolutely and opened up the ion access. The pure PPy electrodes exhibit 25% capacitance retention. The $ZnCo_2O_4$/PPy composite electrodes display 90% capacitance retention after 5000 cycles, which is quite superior to that of PPy nanofilms and is better than the reported cycling stability of PPy/MnO_2 (about 54% after 500 cycles),[44] V_2O_5-PPy (80% after 5000 cycles),[45] and ZnO/PPy (88% after 5000 cycles), [46] Fig. 4e inset shows the 1st and the 5000st GCD curves of charge-discharge cycling tests at the scan rate of 2 mA/cm^2. After 5000 cycles, the shape of curve almost unchanged compared with the 1st cycling curve, indicating stable electrochemical properties of the active material. Such superior cycling stability of hierarchical $ZnCo_2O_4$/PPy nanostructures can be mainly ascribed to the enhanced adherent force between electrode materials and Ni foam by means of $ZnCo_2O_4$ nanowires,[26,47] the electrode fragments held together, and the improved stability of PPy. These results indicate excellent electrochemical stability and good reversible redox behaviors, which have huge application potential in supercapacitors.

Fig. 4f shows the Nyquist plots of the EIS spectra for the PPy, $ZnCo_2O_4$, and

$ZnCo_2O_4$/PPy hybrid electrodes and the inset shows expanded view in the high- and mid-frequency region. At the high frequency, the intersection of the curve at the real part indicates the resistance of the electrochemical system (Rs, which includes the inherent resistance of the electroactive material, ionic resistance of electrolyte, and contact resistance at the interface between electrolyte and electrode). From this picture, the Rs for $ZnCo_2O_4$/PPy is smaller than others (which was measured to be 0.31, 0.37,and 0.30 Ω for PPy, $ZnCo_2O_4$ and $ZnCo_2O_4$/PPy respectively.) The charge&transfer resistance (Rct) of the $ZnCo_2O_4$/PPy is obviously smaller than that of the bare $ZnCo_2O_4$ and PPy, suggesting that the hybrid electrode is beneficial to accelerate the charge transfer. In the low frequency area, the slope of the curve shows the Warburg resistance (Zw), which represents the electrolyte diffusion to the electrode surface.[48] A more ideal straight line (a larger straight-line slope arises from low frequency) can be observed for $ZnCo_2O_4$/PPy than that for $ZnCo_2O_4$ and PPy, indicating the improved capacitive properties for the hybrid.[49,50] By contrast, $ZnCo_2O_4$/PPy displays smallest Rct in addition to the small Rs, indicating the best electrical conductivity and electroactivity.

The two-electrode supercapacitor geometry has been suggested to be the best indication of an electrode material's performance.[51] Fig. 5a shows the CV curves of the hierarchical $ZnCo_2O_4$/PPy nanostructures at various scanning rates ranging from 5-100 mV/s in a potential window of -0.8 V to +0.8 V. The reduction and oxidation peaks on CV curves can be observed and the peak current almost linearly increases with increasing scan rate, in agreement with the trend revealed by the three-electrode system. GCD measurements were further performed at various current densities of 2, 5, 10, 15 and 20 mA/cm^2 and the resultant profiles are given in Fig. 5b. The CV curves and GCD curves of PPy and $ZnCo_2O_4$ were also measured in two-electrode system for comparison (Fig. S5†). Specific energy and specific power are two key factors to evaluate the power applications of electrochemical supercapacitors, which were calculated from the discharge curves according to the equation (3) and (4), respectively. The energy density and power density performance of PPy, $ZnCo_2O_4$,

and $ZnCo_2O_4$/PPy electrodes are shown in Fig. 5c. Obviously, the $ZnCo_2O_4$/PPy hybrid electrodes have the best energy density and power density performance. As seen from the Ragone plots, as the power density increases from 0.5 kW/kg to 5.8 kW/kg when the current density increases from 2 to 20 mA/cm^2, while the energy density decreases from 30.9 to 27.5 Wh/kg. These values are remarkable compared to the most reported electrode materials, such as $ZnCo_2O_4$ electrode[52] with energy density of 12.5 Wh/kg when power density is 0.8 kW/kg at 1.2 mA/cm^2, PPy@MoO_3//AC(+) device[53] with an energy density of 20 Wh/kg when power density is 0.75 kW/kg, CNT@PPy@MnO_2 electrode[54] with the maximum energy density and power density are 8.6 Wh/kg and 16.5 KW/kg. The results demonstrate that the $ZnCo_2O_4$/PPy hybrid materials have excellent electrochemical properties of high energy density and power output in hybrid vehicle systems.

The excellent electrochemical performance can be due to following reasons：(1) The dramatic performance improvement after PPy integration can first be attributed to the smaller Rs (0.30 vs 0.37 Ω) and diffusion resistance of the $ZnCo_2O_4$/PPy hybrid electrode as compared to the pure $ZnCo_2O_4$ electrode in the Fig. 5f. Intimately covered PPy increases both the electrical conductivity of each $ZnCo_2O_4$ nanowire and the electrical contact of $ZnCo_2O_4$ with nickel foam current collector, leading to the maximum utilization of $ZnCo_2O_4$ during the electrochemical reactions.[30] (2) Secondly, we believe that $ZnCo_2O_4$ nanowires can in reverse serve as efficient scaffold to ensure the fine distribution of PPy at nanoscale, making them fully electrochemically accessible, and enhance adherent force between electrode materials and Ni foam to hold the PPy electrode fragments together. (3) In addition, the porous structure of nanowires and nanofilms not only provided more electroactive sites for the Faradic reactions, but also shortened the distance of OH ion/electron transformation, which led to faster kinetics and enhanced electrochemical performance.[55] (4) $ZnCo_2O_4$ nanowires and PPy nanofilms were connected with each other to form a nanoarray network, thus the void space can buffer the volume change during the GCD processes, which has led to enhanced stability of $ZnCo_2O_4$/PPy nanostructures，and the contact

resistance of the whole electrode could be reduced. Secondly, staggered and separated growth of nanofilms not only reduced the free space on the surface of Ni substrate but also increased the effective contact area between electrode and electrolyte, which significantly improved the utilization of active materials.[55] Thus, the synergetic contribution from the two promising pseudocapacitive materials ($ZnCo_2O_4$ and PPy) together with the merits of porous nanoarray network architecture[56] should account for the exceptionally high capacitance and better rate capability of the $ZnCo_2O_4$/PPy hybrid electrode, which are encouraging since our electrode is entirely carbon additive- and binder-free.

Conclusions

$ZnCo_2O_4$/PPy hybrid electrodes are successfully synthesized on Ni foam. They exhibited a prominent electrochemical performances of 1559 F/g at 2 mA/cm^2 and a high energy density of 30.9 Wh/kg at a power density of 0.2 kW/kg. After charging/discharging for 5000 cycles at a high current density of 10 mA/cm^2, 90% of the initial specific capacitance was retained. Such promising electrochemical stability mainly attributed to the $ZnCo_2O_4$ nanowires that enhanced adherent force between electrode materials and Ni foam and hindered the structural degradation of the polymer. In addition, good electrical conductivity rendered by PPy integration, in combination with facile ion diffusion path provided by both the porous structures of PPy nanofilms and $ZnCo_2O_4$ nanowires, give rise to enhanced rate capability. Our work opens up the possibility to engineer $ZnCo_2O_4$/PPy hybrid nanostructures into a promising pseudocapacitive material.

Acknowledgements

This work was partially supported by the Natural Science Foundation of China (Nos. 51277044).

Reference

1 A. Rudge, J. Davey, I. Raistrick, S. Gottesfeld and J. P. Ferraris, *J. Power Sources*, 1994, **47**, 89.

2 X. Peng, L. Peng, C. Wu and Y. Xie, *Chem. Soc. Rev.*, 2014, **43**, 3303.

3 M. Winter and R.J. Brodd, *Chem. Rev.*, 2004, **104**, 4245.

4 L. Huang, D. C. Chen, Y. Ding, S. Feng, Z. L. Wang and M. L. Liu, *Nano Lett.*, 2013, **13**, 3135.

5 X.Y. Cao, X. Xing, N. Zhang, H. Gao, M.Y. Zhang, Y.C. Shang and X.T. Zhang, J. Mater. Chem. A, 2015, **3**, 3785.

6 H. Shirakawa, E. J. Louis, A. G. MacDiarmid, C. K. Chiang and A. J. Heeger, *J. Chem. Soc., Chem. Commun.*, 1977, 578.

7 A. K. Bakhshi and G. Bhalla, *J. Sci. Ind. Res.*, 2004, **63**, 715.

8 K. Jurewicz, S. Delpeux, V. Bertagna, F. Beguin and E. Frackowiak, *Chem. Phys. Lett.*, 2001, **347**, 36.

9 T. E. Campbell, A. J. Hodgson and G. G. Wallace, *Electroanalysis*, 1999, **11**, 215.

10 S. Kuwabata, J. Nakamura and H. Yoneyama, *J. Electrochem. Soc.,*1990, **137**, 2147.

11 H. F. An, Y. Wang, X.Y. Wang, L. P. Zheng, X. Y. Wang, L. H. Yi, L. Bai and X. Y. Zhang, *J. Power Sources.*, 2010, **195**, 6964.

12 C. Meng, C. Liu, L. Chen, C. Hu and S. Fan, *Nano Lett.*, 2010, **10**, 4025.

13 G. Zhang and X. W. Lou, *D. Adv. Mater.,* 2013, **25**, 976.

14 G. Wang, L. Zhang and J. Zhang, *Chem. Soc. Rev.,* 2012 , **41**, 797.

15 S. T. Selvan, J. P. Spatz, H. A. Klok and M. Moller, *Adv.Mater.*, 1998 ,**10** ,132.

16 L. Qiu, Y. Peng, B. Liu, B. lin, Y. Peng, M. J. Malik and F. Yan, *Appl. Catal. A*, 2012, **230**, 413.

17 W. K. Chee, H. N. Lim, I. Harrison, K. F. Chong and Z. Zainal, C. H. N, N. M. Huang, T. Fu, W. J. Ren, J. D. Li and Q. H. Li, *J. Mater. Chem. A,* 2014, **2**, 16116.

18 V. Branzoi, F. Branzoi and L. Pilan, *Mater. Chem. Phys.*, 2009, **118**, 197.

19 M. Davis, C. Guemeci, B. Black, C. Korzeniewski and L. Hope-Weeks, *RSC Adv.,*

2012, **2**, 2061.

20 X. Song, Q. Ru, B. B. Zhang, S. J. Hu and B. N. An, *Journal of Alloys and Compounds*., 2014, **585**, 518.

21 G. Zhou, J. Zhu, Y. J. Chen, L. Mei, X. C. Duan, G. H. Zhang, L. B. Chen, T. H..Wang and B. G. Lu, *Electrochimica Acta.* 2014, **123**, 450.

22 H. Wu, ZH. Lou, H. Yang and G. ZH. Shen, *Nanoscale*, 2015, **7**, 1921.

23 S. Chen , M. Xue, Y. Q. Li, Y. Pan, L. K. Zhu, D. L. Zhang, Q. R. Fang and S. L. Qiu, *Inorg. Chem. Front.*, 2015, **2**,177.

24 B. Liu, B. Y. Liu, Q. F. Wang, X. F. Wang, Q. Y. Xiang, D. Chen and G. Z. Shen, *ACS Appl. Mater. Interfaces*, 2013, **5**, 10011.

25 B. K. Guan, D. Guo, L. L. Hu, G. H. Zhang, T. Fu, W. J. Ren, J. D. Li and Q. H. Li, *J. Mater. Chem. A*, 2014, **2**, 16116.

26 H. X. Chuo, H. Gao, Q. Yang, N. Zhang, W. B. Bu and X. T. Zhang. *J. Mater. Chem. A*, 2014, **2**, 20462.

27 S. B. Wang, J. Pu, Y. Tong, Y. Y. Chen, Y. Gao and Z. H. Wang, *J. Mater. Chem. A.*, 2014, **2**, 5434.

28 Q. H. Wang, L. X. Zhu, L. Q. Sun, Y. C. Liu and L. F. Jiao, *J. Mater. Chem. A*, 2015, **3**, 982.

29 L. Z. Fan and J. Maier, *Electrochemistry Communications*, 2006, **8**, 937.

30 G. J. Cruz, M. G. Olayo, O. G. López, L. M. Gómez, J. Morales and R. Olayo, *Polymer*. 2010, **51**, 4314.

31 P. Heyse, R. Dams, S. Paulussen, K. Houthoofd, K. Janssen and P. A. Jacobs, et al, *Plasma Process Polym*. 2007, **4**, 145.

32 C. Zhou, Y. W. Zhang, Y. Y. Li and J. P. Liu, *Nano Lett.*, 2013, **13**, 2078.

33 B. B. Yue, C. Y. Wang, X. Ding and G. G. Wallace, *Electrochim. Acta*, 2012, **68**, 18.

34 D. Zhang, Q.Q. Dong, X. Wang, W. Yan, W. Deng and L.Y. Shi, *J. Phys. Chem. C*, 2013, **117**, 20446.

35 X. Zhang, W. S. Yang and Y. W. Ma, *Electrochem. Solid-State Lett.,* 2009, **12**, A95.

36 G. F. Ma, H. Peng, J. J. Mu, H. H. Huang, X. Z. Zhou and Z. Q. Lei, *Journal of Power Sources*, 2013, **229**, 72.

37 X. J. Ma, L. B. Kong, W. B. Zhang, M. C. Liu, Y. C. Luo and L. Kang, *RSC Adv.*, 2014, **4**, 17884.

38 D. P. Cai, D. D. Wang, B. Liu, L. L. Wang, Y. Liu, H. Li, Y. R. Wang, Q. H. Li and T. H. Wang, *ACS Appl. Mater. Interfaces*, 2014, **6**, 5050.

39 T. Y. Liu, L. Finn, M. H. Yu, H. Y. Wang, T. Zhai, X. H. Lu, Y. X. Tong and Y. Li, *Nano Lett.*, 2014, **14**, 2522.

40 B. Muthulakshmi, D. Kalpana, S. Pitchumani and N. G. Renganathan. *Journal of Power Sources*, 2006, **158**, 1533.

41 T. Qian, N. Xu, J. Q. Zhou, T. Z. Yang, X. J. Liu, X. W. Shen, J. Q. Liang and C. L. Yan, *J. Mater . Chem. A*, 2015, **3**, 488.

42 B. Liu, B. Y. Liu, Q. F. Wang, X. F. Wang, Q. Y. Xiang, D. Chen and G. Z. Shen. *ACS Appl. Mater. Interfaces*, 2013, **5**, 10011.

43 B. K. Guan, D. Guo, L. L. Hu, G. H. Zhang, T. Fu, W. J. Ren, J. D. Li and Q. H. Li, *J. Mater. Chem. A.*, 2014, **2**, 16116.

44 A . Bahloul, B. Nessark, E. Briot, H. Groult, A . Mauger, K. Zaghib, C.M. Julien，*Journal of Power Sources*, 2013, **240**, 267.

45 M. H. Bai, L. J. Bian, Y. Song, and X. X. Liu, *ACS Appl. Mater. Interfaces*.2014, **6**, 12656.

46 N. K. Sidhu, and Rastogi, *Nanoscale Research Letters,* 2014, **9**, 453.

47 G. W. Yang, C. L. Xu and H. L. Li, *Chem. Commun.*, 2008, 6537.

48 X. Y. Liu, S. J. Shi, Q. Q. Xiong, L. Li, Y. J. Zhang, H. Tang, C. D. Gu, X. L. Wang and J. P. Tu, *ACS Appl. Mater. Interfaces*, 2013, **5**, 8790.

49 A. Davies, P. Audette, B. Farrow, F. Hassan, Z. Chen, J. Y. Choi and A. Yu, *J. Phys. Chem. C*, 2011, **115**, 17612.

50 H. H. Chang, C. K. Chang, Y. C. Tsai and *C. S.* Liao, *Carbon,* 2012, **50**, 2331.

51 M. D. Stoller and R. S. Ruoff, *Energy Environ. Sci.*, 2010, **3**, 1294.

52 S. B. Wang, J. Pu, Y. Tong, Y. Y. Chen, Y. Gao and Z. H. Wang, *J. Mater. Chem. A*, 2014, **2**, 5434.

53 Y. Liu, B. Zhang, Y. Yang, Z. Chang, Z. Wen and Y. Wu, *J.Mater. Chem. A,* 2013, **1**, 13582.

54 P. X. Li, Y. B. Yang, E. Z. Shi, Q. C. Shen, Y. Y. Shang, S. T. Wu, J. Q. Wei, K. L. Wang, H. W. Zhu, Q. Yuan ,A. Y. Cao and D. H. Wu, *ACS Appl. Mater. Interfaces,* 2014, **6**, 5228.

55 F. X. Bao, X. F. Wang, X. D. Zhao, Y. Wang, Y. Ji, H. D. Zhang and X. Y. Liu, *RSC Adv.*, 2014, **4**, 2393.

56 J. Jiang, Y. Y. Li, J. P. Liu, X. T. Huang, C. Z.Yuan, and X. W. Lou, *Adv. Mater.* 2012, **24**, 5166.

Figure Captions:

Fig. 1. The representative synthetic procedure and structure details of the hybrid nanostructure electrode.

Fig. 2. (a) Low and (b)、(c) high-magnification SEM images of $ZnCo_2O_4$ nanowires. (d) Low and (e)、(f) high-magnification SEM images of the hierarchical $ZnCo_2O_4$/PPy nanostructures.

Fig. 3. (a) TEM and (b) HRTEM images of the $ZnCo_2O_4$ nanowires. (c) TEM and (d) HRTEM images of the $ZnCo_2O_4$/PPy nanostructures. (e) FTIR spectrum of the $ZnCo_2O_4$/PPy hybrid nanostructures. (f) XRD pattern of the $ZnCo_2O_4$, $ZnCo_2O_4$/PPy hybrid nanostructures grown on Ni foam.

Fig. 4. (a) CV curves of the PPy, $ZnCo_2O_4$, $ZnCo_2O_4$/PPy hybrid electrodes at a scan rate of 25 mV/s. (b) CV curves of $ZnCo_2O_4$/PPy hybrid electrodes at various scan rates. (c) GCD curves of $ZnCo_2O_4$/PPy hybrid electrodes at various current densities. (d) Specific capacitances for PPy, $ZnCo_2O_4$, $ZnCo_2O_4$/PPy as a function of the current density. (e) Cycling performances of PPy, $ZnCo_2O_4$, $ZnCo_2O_4$/PPy during 5000 cycles at a current density of 10 mA/cm^2. The inset shows that the shape of GCD curves for the last cycle has small change compared with the 1st cycling curve for $ZnCo_2O_4$/PPy. (f) EIS spectra of the PPy, $ZnCo_2O_4$, $ZnCo_2O_4$/PPy hybrid electrodes, respectively. Inset shows the magnification part of high frequency range for the EIS spectra.

Fig. 5. (a) CV and (b) GCD curves of $ZnCo_2O_4$/PPy hybrid electrodes at various scan rates and current densities in a two electrode system, respectively. (c) Energy and powder densities of the PPy, $ZnCo_2O_4$, $ZnCo_2O_4$/PPy hybrid electrodes in a two electrode system.

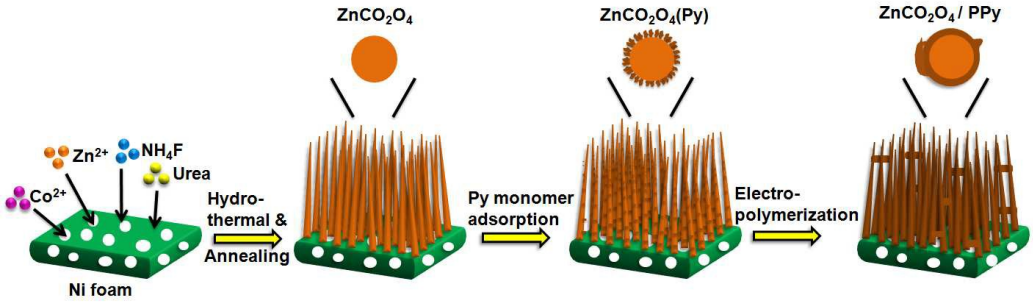

Fig. 1. by T. T. Chen, et al.

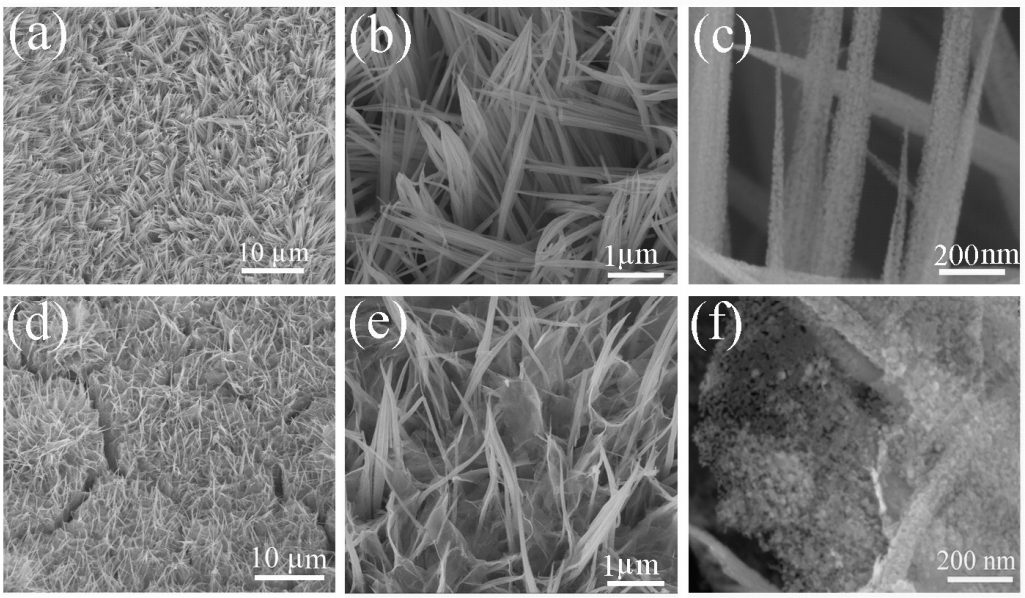

Fig. 2. by T. T. Chen, et al.

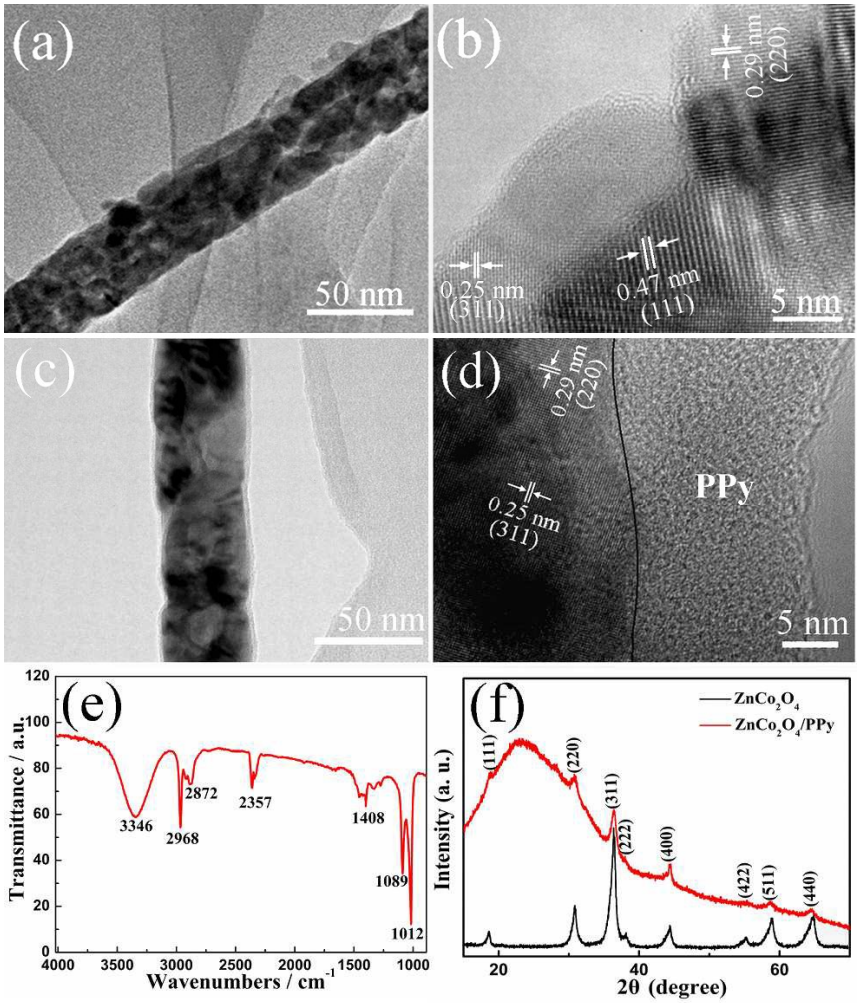

Fig. 3. by T. T. Chen, et al.

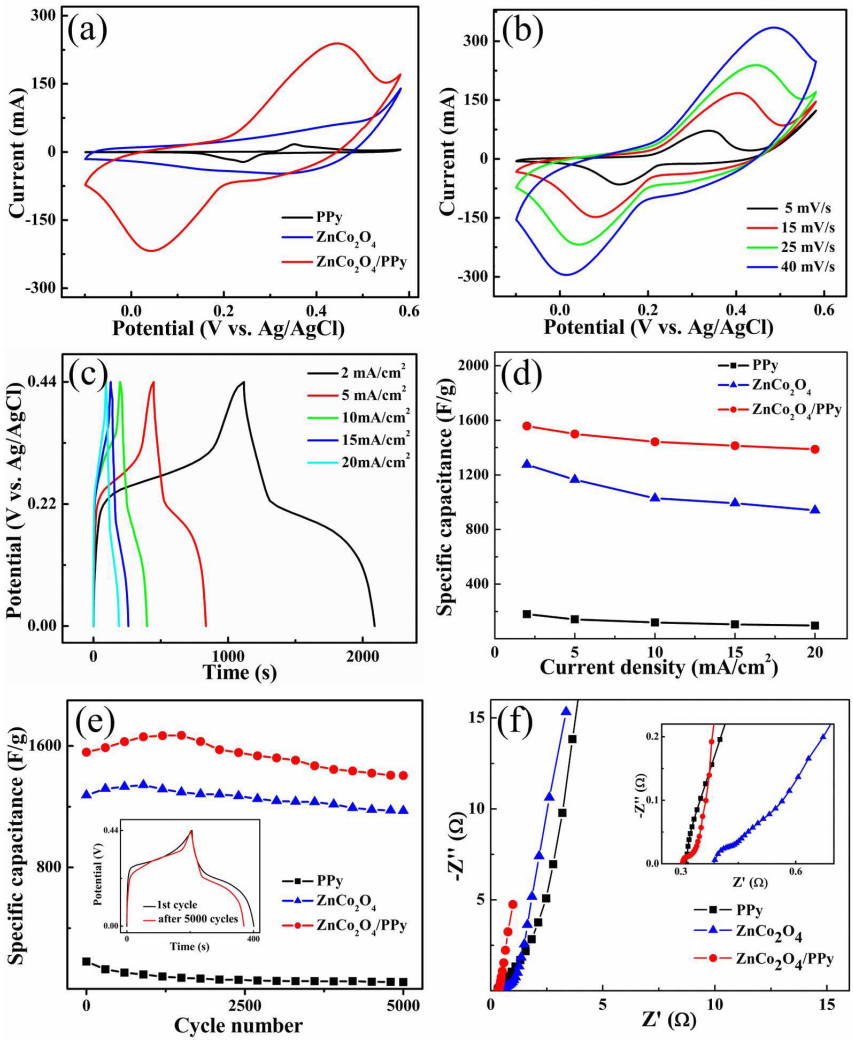

Fig. 4. by T. T. Chen, et al.

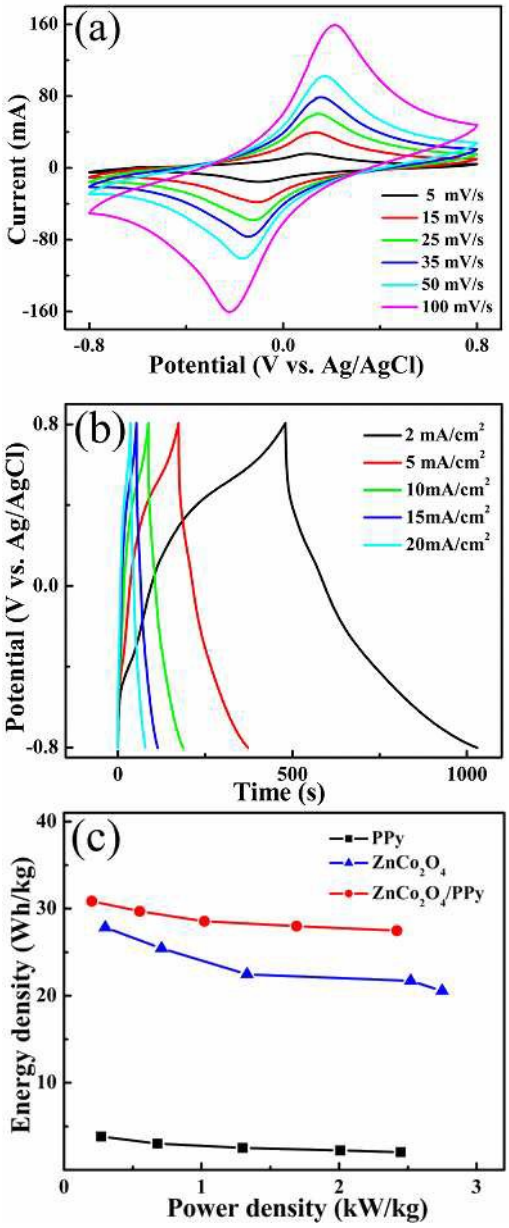

Fig. 5. by T. T. Chen, et al.

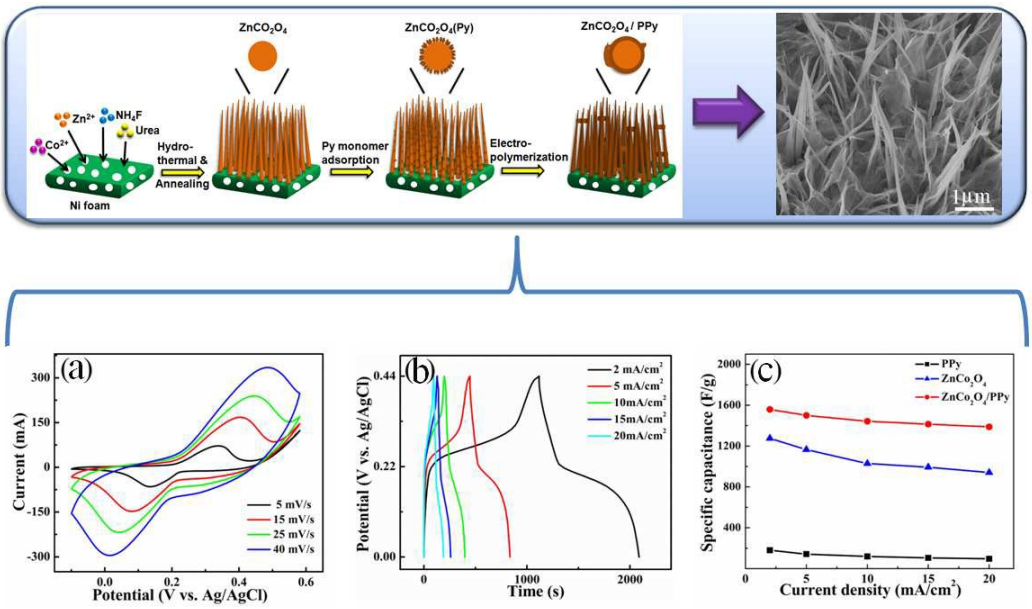

The synthesis procedure of $ZnCo_2O_4$/PPy composite electrodes and the electrochemical properties of the composite electrodes.